Cell Reports
Physical Science

CellPress
OPEN ACCESS

Article

Spatiotemporal Control of Electrochemiluminescence Guided by a Visible Light Stimulus

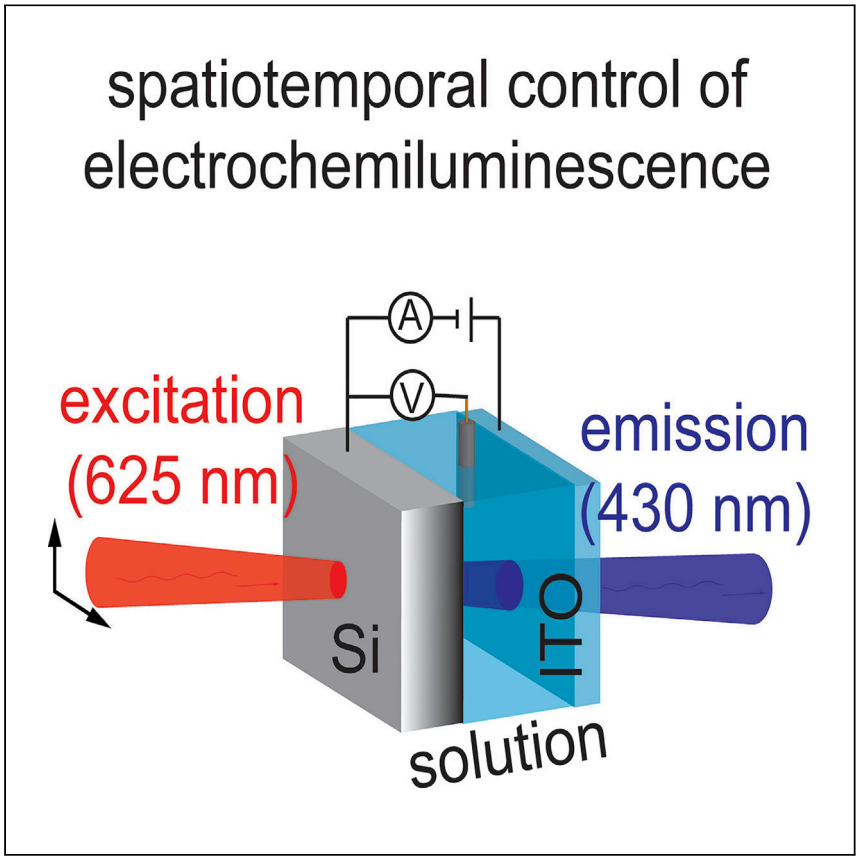

Vogel et al. report the spatiotemporal control of chemiluminescence by means of locally modulating, with light, the kinetics of a redox reaction that initiates the chemical path to a light-emitting species. The excitation light is not required to pass through the liquid sample, providing a strategy to excite a luminophore under dark conditions.

Yan B. Vogel, Nadim Darwish, Simone Ciampi

simone.ciampi@curtin.edu.au

HIGHLIGHTS

Photoelectrochemical generation of an excited-state light emitter

Spatiotemporal control of chemiluminescence is demonstrated

Spatiotemporal control of electrochemiluminescence by modulation of surface conductivity

The liquid sample is kept under dark, preventing damages of photosensitive specimens

Vogel et al., Cell Reports Physical Science *1*, 100107
July 22, 2020
https://doi.org/10.1016/j.xcrp.2020.100107

Cell Reports
Physical Science

CellPress
OPEN ACCESS

Article

Spatiotemporal Control of Electrochemiluminescence Guided by a Visible Light Stimulus

Yan B. Vogel,[1] Nadim Darwish,[1] and Simone Ciampi[1,2,*]

SUMMARY

Chemiluminescence and fluorescence have revolutionized the study of chemical and biological processes. However, unlike fluorescence, spatiotemporal control of chemiluminescence is challenging, and the technically simple solution of converting chemical energy into light energy only at specific sites defined by a clean, easy-to-deliver focused light stimulus is not yet a viable option. Here, we demonstrate the spatial and temporal control of a chemiluminescent reaction by photoinduced oxidative hotspots on a silicon surface. The excitation light is not required to pass through the liquid sample; hence, the light stimulus can excite a luminescent dye under effectively dark conditions. This provides a strategy for removing light-induced sample damages, photobleaching, and autofluorescence.

INTRODUCTION

Much of our understanding of biological processes has come from developing and applying microscopy techniques that harness light emission associated with chemical changes.[1–6] Fluorescence remains the dominant microscopy technique.[4–6] However, two of the major drawbacks of fluorescence—autofluorescence, and the risk of damaging light-sensitive samples—are absent in chemiluminescence, potentially giving it a significant advantage over fluorescence in the field of microscopy.[7] Control in 2D and over time of chemiluminescence requires control of a chemical stimulus, but such level of control has not yet been demonstrated.

Here, we address in space and time a chemiluminescent emission by harnessing localized, light-addressable, microscopic electron-sink sites on a macroscopic semiconductor surface. We take advantage of the photoelectric properties of silicon to localize transient fluxes of charge carriers at an illuminated silicon-electrolyte interface.[8] This opens up the possibility of a electrogenerated chemiluminescent output that is (1) of shorter wavelength than the excitation source;[9] and (2) controlled with a degree of spatial and temporal resolution not otherwise possible either by chemical means,[1,10] or by using an array of electrodes.[11,12] Since light is merely used to generate localized and microscopic oxidative hotspots on a macroscopic electrode, the excitation light can therefore impinge the silicon "dry" backside, while the "wet" face in contact with the sample is kept under dark conditions, hence effectively using the light stimulus to excite a luminescent dye under dark conditions.

At a semiconductor-liquid interface a thin space charge layer extends inside the solid.[13] Depending on the externally applied voltage, this near-surface layer can be depleted or accumulated of charge carriers.[13] When the interface is biased into its depletion regime, the space charge layer becomes highly resistive, and

[1]School of Molecular and Life Sciences, Curtin Institute of Functional Molecules and Interfaces, Curtin University, Bentley, WA 6102, Australia

[2]Lead Contact

*Correspondence: simone.ciampi@curtin.edu.au

https://doi.org/10.1016/j.xcrp.2020.100107

charge transfer across the interface is impeded.[13] In the case of a depleted n-type photoanode, as depicted in Figure 1A, photogenerated holes accumulate in the valence band and are collected by reduced luminol molecules (5-amino-2,3-dihydrophthalazine-1,4-dione) present in the electrolyte. The main reactions (redox and non-redox) involved in the design of our photoinduced electrochemiluminescent system are schematized in Figure 1B. The monoanion of luminol (at the pH studied in this work luminol is present in the form of its monoanion)[14] is first oxidized by one photogenerated hole to diazasemiquinone radical (i) and then reacts with a superoxide radical in a nucleophilic addition forming a bicyclic endoperoxide (ii).[15] Nitrogen loss leads then to an excited state intermediate, 3-aminophtalate*, which in water emits blue light (425 nm) upon relaxation (iii and iv).[15] The superoxide radical comes principally from the oxidation of HO_2^- present in the alkaline aqueous solution.

With the objective of exploring to what degree a localized flux of photogenerated surface holes translates to a localized chemiluminescence emission (Figure 1C), we spatiotemporally address the light stimulus impacting the semiconductor using an adaptation of a ferroelectric liquid crystal spatial light modulator (Figure 1D).[16] This type of spatial light modulation, often used in super resolution microscopy,[17] allows projecting over an electrified macroscopic substrate any arbitrary user-defined image, or sequence of images. This gives high spatial and temporal resolution of the light stimulus (in the current setup these are, respectively, 4 μm and 4.5 kHz), with a 2D flexibility[18,19] not otherwise possible using a traveling light pointer.[20] A dichroic mirror reflecting wavelengths below 550 nm is placed between the semiconductor and the incoming light, so that the supra band gap red radiation (625 or 730 nm) can reach the electrode to address its conductivity, while any higher-energy emission (Figure 2A) is reflected toward a complementary metal-oxide-semiconductor (CMOS) camera. This setup can therefore operate with both front and backside electrode excitations (Figure 1D), with the latter being investigated here to demonstrate a method of removing light exposure to the sample.

RESULTS AND DISCUSSION

ON-OFF Switch of Electrochemiluminescence by Light

Before attempting to localize the electrochemiluminescence of luminol in 2D, we first sought to demonstrate the ON-OFF switch of the luminescence across the entire macroscopic electrode surface. For this purpose, we illuminated the entire silicon-electrolyte interface (~0.28 cm^2). Luminol electrogenerated chemiluminescence is generally reported for anodically biased metals.[21] Because of difficulties in preventing anodic decomposition of non-oxide semiconductors,[22] electrogenerated chemiluminescence has only been reported for silicon surfaces coated with a passivating thin metallic layer.[9] However, while a protective metallic layer is an effective solution to prevent substrate oxidation, its presence will eliminate any possibility of gaining lateral resolution for a light-activated charge transfer process. On the contrary, Si-C-bound monolayers of 1,8-nonadiyne molecules, effectively both prevent corrosion of the silicon photoelectrode,[22] as well as ensure negligible in-plane electrical conduction.[23,24] Representative optical measurements, such as those in Video S1, reveal a stable electrochemiluminescence emission from low doped n-type silicon photoanodes under frontside illumination.

The choice of proceeding first by validating the experimental design under frontside illumination was to ensure a maximum flow of holes to the reaction site, hence the largest possible chemiluminescent output. Alternatively, using backside illumination

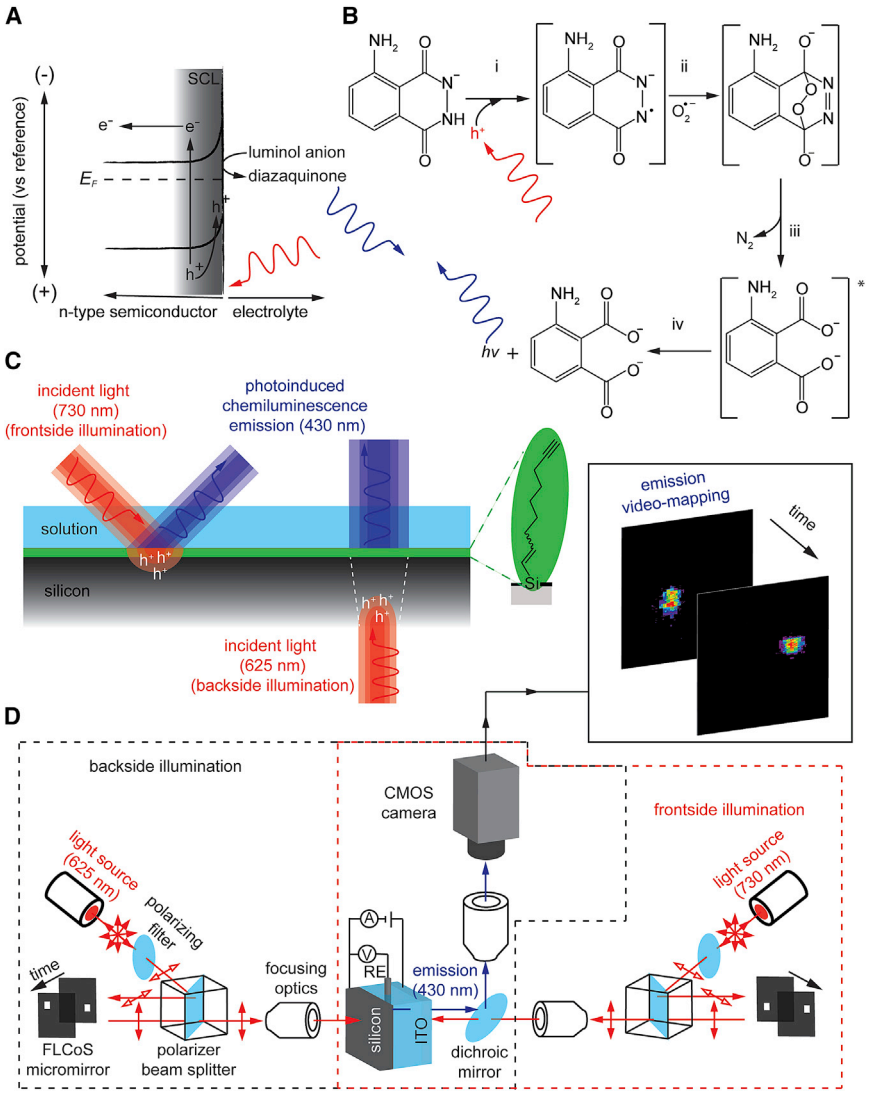

Figure 1. Spatiotemporal Control of Electrochemiluminescence at a Macroscopic and Unstructured Semiconductor Surface

(A) Band diagram of an illuminated n-type semiconductor under reverse bias (depletion). Incident photons with energy greater than the band gap (red wavy arrows) create electron/holes pairs (e^-/h^+). The electric field present in the space charge layer (SCL) drives electrons to the semiconductor bulk and holes to the liquid interface. Holes are captured by a luminol molecule to yield a diazasemiquinone radical intermediate.

(B) Proposed mechanism for the photoinduced anodic electrogenerated chemiluminescence of luminol. The monoanion of luminol is first oxidized to diazasemiquinone radical (i), which reacts with superoxide radical in a cycloaddition reaction (ii), resulting in the formation of the excited state 3-aminophtalete*, which emits light upon relaxation (iii and iv).

(C) Schematics depicting the monolayer chemistry and the spatiotemporal control of electrochemiluminescence in either front (left) or backside (right) illumination mode.

(D) The 2D spatial modulation of the light beam addressing the conductivity of the silicon electrode is accomplished by a micromirror array of ferroelectric liquid crystal elements on silicon (FLCoS). Sequences of user-defined images (arrays 3.1 million of ON-OFF pixels) are projected on the semiconductor substrate. Each element of the FLCoS micromirror can either change (ON pixels, depicted in white) or leave unchanged (OFF pixels, depicted in black) the polarization of the light reflected toward the semiconductor substrate. The presence of a polarizer beam splitter between the FLCoS and the semiconductor creates an "ON pixels only" image on the latter. The incident red image (730 nm or 625 nm) addresses in 2D a chemiluminescent blue (430 nm) emission. Emission frames are collected by a CMOS camera.

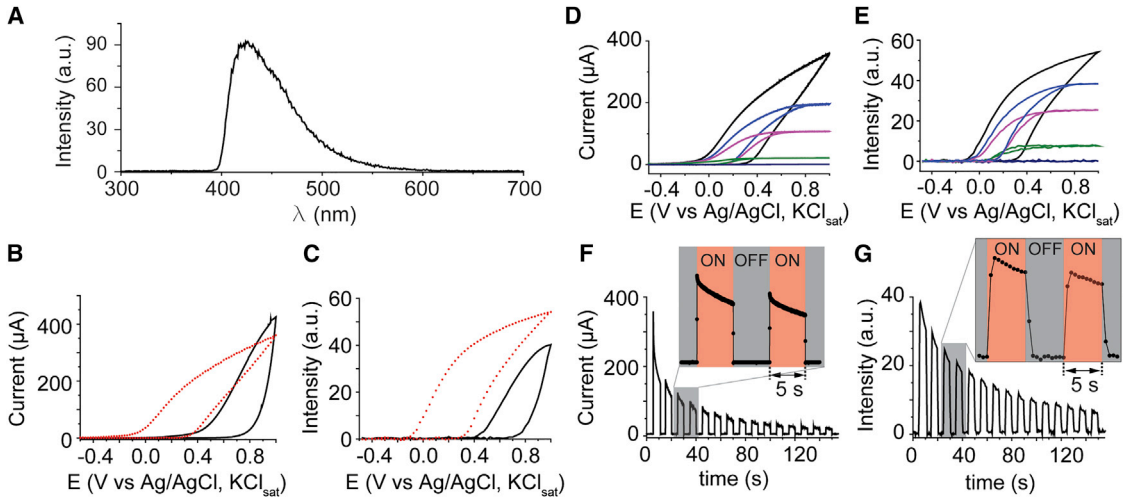

Figure 2. ON-OFF Switch of Electrochemiluminescence by Visible Light

(A) Electrogenerated chemiluminescence emission spectra of luminol obtained on a highly doped (HD) silicon electrode biased at +0.8 V (versus Ag/AgCl, KCl_{sat}).

(B and C) Electrochemical (B) current-voltage and (C) luminescence emission intensity-voltage curves. Data were recorded using either HD (black solid line) or low doping (LD) silicon electrodes (red symbols).

(D and E) Effect of the incident light intensity (max, black; max/3.6, blue; max/5.1, magenta; max/8.5, green; 0, indigo) on the electrochemical current-voltage (D) and luminescence emission intensity-voltage (E) curves obtained on LD electrodes.

(F and G) Representative amperometric (F) and light emission (G) traces demonstrating the ON-OFF switch of the luminol electrochemiluminescence under a chopped light source addressing the silicon conductivity. The time decay, of both the current (F) and the light intensity (G), has a mass transport origin.

Experiments in (A–G) were performed using Si(111) electrodes modified with a protecting monolayer of 1,8-nonadiyne, and in the presence of 5.0×10^{-2} M luminol, 1.0×10^{-1} M potassium hydroxide, and 1% (v/v) H_2O_2. In (B–E) the voltage scan rate was 50 mV/s. The amperometric curves in (F) and (G) were performed under a constant voltage of +0.2 V (versus Ag/AgCl, KCl_{sat}) at constant light intensity. Substrate illumination of LD silicon is by means of a frontside deep red radiation (730 nm). Experiments for the HD silicon were performed under dark conditions.

and therefore forcing a longer diffusion path for photogenerated holes, would have led to a loss of oxidative power (vide infra). Furthermore, changes to the intensity of the incident illumination were expected not only to affect the luminescence intensity but also the voltage required to generate it. The electrogenerated chemiluminescence of luminol on metals or "metallic" highly doped semiconductors requires relatively large positive voltages (>0.4 V; black solid lines in Figures 2B and 2C) but on a low doped semiconductor extra oxidative power is supplied by the incident photons (Figure 1A). The result is that on depleted and illuminated n-type Si light emission is triggered at a record low voltage of −0.2 V (Figures 2B and 2C, red dotted line). The advantage of using photoelectrochemistry at silicon to trigger a chemiluminescent reaction at contrathermodynamic voltages has also been recently reported for the oxidation of $[Ru(byp)_3]^{2+}$.[9] We remark that in absence of an externally applied potential there is no luminescence emission.

In more details, Figures 2D and 2E show the influence of both light intensity and bias on electrochemical currents and luminescence emission. As the intensity of the incident red light increases, the open circuit voltage shifts to less anodic values, in proportion to the logarithm of $I_0/(I_0 + I_L)$, where I_0 and I_L are the reverse-saturation diode current and the photogenerated current, respectively.[25] The contrathermodynamic shift observed for the onset of luminescence parallels the shift of the system open circuit voltage, and, as the incident light intensity increases, the 430 nm emission is observed under less anodic voltages. It can also be inferred from the current-voltage and emission intensity-voltage data in Figures 2D and 2E that both oxidation rates and electrochemiluminescence intensities reach a plateau when the incident

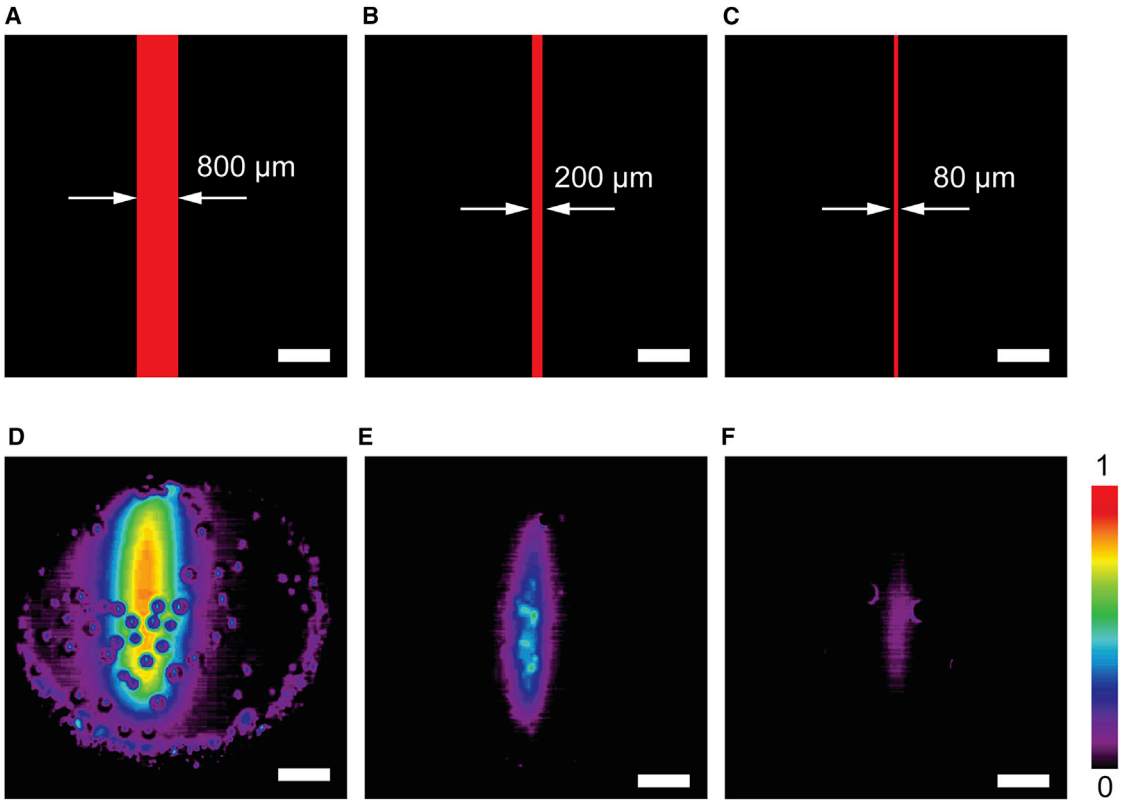

Figure 3. Spatial Resolution of Electrochemiluminescence

(A–F) By projecting user-defined images, luminol oxidation and its electrogenerated electrochemiluminescence are spatially confined on a silicon photoanode. (A)–(C) show the shape of the supra band gap light (730 nm) reaching the silicon-electrolyte interface, and (D)–(F) show the corresponding false-color electrochemiluminescence intensity emission microscopy images. The intensity bar is in arbitrary units. The white ink labels specify the width of the line-shaped illumination pattern. The substrate is low-doped n-type Si(111), modified with a protecting monolayer of 1,8-nonadiyne. A constant voltage of +0.8 V (versus Ag/AgCl, KCl_{sat}) is applied to the Si(111), while microscopy images are taken with a 200 ms exposure time. The electrolyte is 1.0×10^{-1} M potassium hydroxide, with 5.0×10^{-2} M luminol, and 1% (v/v) H_2O_2. Substrate illumination is by means of a frontside deep red radiation (730 nm). Scale bars are 1 mm.

light is sufficiently low. This steady state is a kinetic effect arising when the current across the interface is limited by the amount of photogenerated charge carriers.[25–28] When the light is turned off, there are only thermal carriers and the semiconductor substrate is of high resistance, and electrochemiluminescence is not observed within the accessible voltage window (Figures 2D and 2E). Furthermore, data in Figures 2F and 2G show how both the electrochemical current and the luminescence emission rapidly track the ON-OFF switching of the light stimulus. The decay in both current and light emission over time has a mass transport origin. The electrochemiluminescence output is stable over time; see Video S1.

Confinement of Electrochemiluminescence by Spatial Light Modulation

After proving the ON-OFF switch of the luminol electrochemiluminescence by means of modulating in time the incident light, we proceeded to investigate the possibility of confining the emission only to a discrete illuminated area, specifically trying to define to what extent electrochemiluminescence can follow a static, or dynamic, illumination pattern. Examples of static illumination patterns are shown in Figures 3A–3C, while Figures 3D–3F are the corresponding false-color intensity luminescence emission microscopy images. The images in Figures 3D–3F show that luminol reactivity, hence its light-output, can be confined to selected areas.

This is exemplified by projecting line-shaped red light patterns (730 nm) of specific widths (80–800 μm) on the frontside of depleted low doped n-type Si electrodes.

Although it is evident that electrochemiluminescence is generally emitted in correspondence of the illuminated area, the match is not perfect. The 2D luminescence profiles are generally broader than the projected images, an effect most likely due to the lateral diffusion of photogenerated carriers. This loss of resolution is not surprising since the minority carriers diffusion length in crystalline silicon is several micrometers.[29] In an attempt to improve spatial resolution, we replaced crystalline with amorphous silicon, the latter having a carrier diffusion length of only few nanometers.[30] We followed the same passivating procedure applied to the hydrogen-terminated crystalline substrates and modified the amorphous silicon layer with a protective 1,8-nonadiyne monolayer. Surprisingly, although the electrochemical oxidation of luminol can still be turned ON and OFF by intermittently illuminating the whole amorphous silicon surface (current-potential responses in Figure S1A), we could not detect any electrochemiluminescence emission with a CMOS camera (Figure S1B). We speculate that this may be due to the relatively low electrochemical signal in amorphous silicon (anodic currents were ~2 orders of magnitude lower than in crystalline Si), which is a result of its high recombination rates. At present, there is therefore evidence of a trade-off between the 2D resolution and the intensity of the emission.

Another feature of the emission micrographs in Figures 3D–3F is that the center of the reaction cell appears consistently to emit brighter luminescence. This is probably an aberration effect due to the field-curvature of the lenses focusing the incident red light. Round spots of low luminescence can also be observed (Figure 3D), which are likely to be sites where oxygen gas bubbles are liberated from hydrogen peroxide decomposition.

Spatiotemporal Control of Electrochemiluminescence by Light

The spatial confinement of electrochemiluminescence, demonstrated in Figure 3, makes it possible to address an up-converted emission, from 730 to 430 nm, at any arbitrary electrode location, and potentially at any given time. The latter feature—time resolution—is shown in Figure 4, where 200 μm wide red light squares are projected in rapid sequence (600 ms) at random x-y locations (Figure 4A) across a macroscopic and unstructured Si electrode. The corresponding optical outputs, shown in Figure 4B, are a proof of principle of a spatiotemporally resolved electrochemiluminescence emission achieved over an electrode that has a single peripheral electrical connection to its voltage source. The temporal resolution is limited by the exposure-time needed to detect the emission, and in our setup this sampling limit was 250 ms (see Figure S2). The high spatiotemporal control of our spatial light modulator design may be of relevance in applications such microscopy, where the study of dynamic biological processes requires a large x-y speed and resolution.[31,32]

Furthermore, as shown in Figure 4 for the sequential illumination of non-adjacent areas, speed constrains generally imposed by a raster scan, such as when mechanical moving probes are involved,[33,34] are completely removed by our spatial light modulation concept. This could allow the observation of processes separated in space but occurring simultaneously, for example, mapping diffusion fronts in viscous electrolytes and/or over rough substrates, which is outside the reach of current redox imaging techniques such as those based on scanning probes.[35,36] Nevertheless, if required, a raster-type scan of the sample, as well as the projection of any arbitrary moving shape, can still be implemented (Videos S2, S3, and S4).

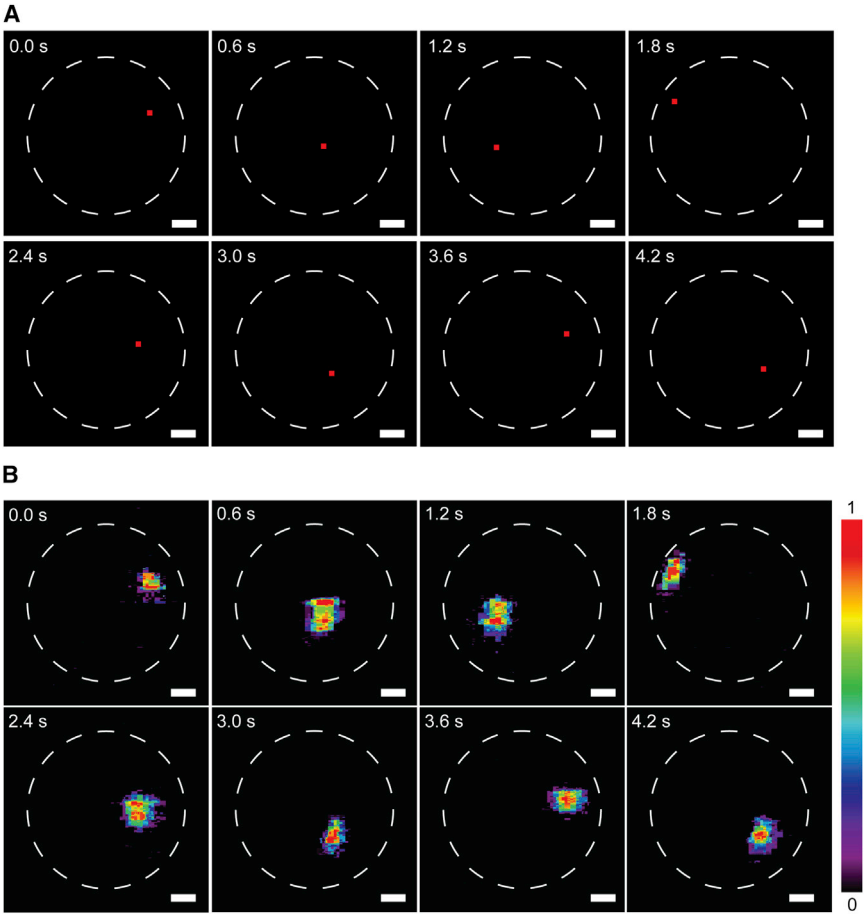

Figure 4. Spatiotemporally Resolved Electrochemiluminescence Emission

(A) A dynamic red-light pattern (730 nm, squares with side of 200 μm) illuminates sequentially specific areas of a macroscopic silicon-electrolyte interface. The electrode is n-type Si(111) of low doping, modified with a protecting monolayer of 1,8-nonadiyne and biased into depletion. The dashed white circles indicate the limit of the interface.

(B) Video frames (false-color intensity, intensity bar is in arbitrary units) showing the 2D mapping of the electrogenerated chemiluminescence emission. The video frame time stamp is specified at the top-left corner of each panel. Electroluminescence images were recorded with an exposure time of 600 ms, such to match the frame rate of the projected dynamic pattern. A constant voltage of +0.8 V (versus Ag/AgCl, KCl_{sat}) is applied to the silicon electrode during the experiment. The electrolytic solution contained 1.0×10^{-1} M potassium hydroxide, 5.0×10^{-2} M luminol, and 1% (v/v) H_2O_2. Substrate illumination is by means of a frontside deep red radiation (730 nm). Scale bars are 1 mm.

Spatiotemporal Control of Electrochemiluminescence under Dark Conditions

The above experiments prove the spatiotemporal control of electrochemiluminescence by using a frontside illumination to generate photocarriers *in silicon* (Figure 1C). As discussed above, illumination of the silicon-electrolyte interface was for having charge carriers trapped by luminol as soon as generated. This arrangement limits lateral hole diffusion, hence theoretically giving higher emissions and better resolutions. However, the possibility of using backside illumination, that is, from the silicon side not in contact with the solution (Figure 1C, right), is attractive if dealing with photosensitive samples. It removes light exposure, and avoids nonspecific signals, major challenges encountered in fluorescence microscopy. To ensure a completely dark wet side, we used an incident light with wavelength of 625 nm, which has a penetration depth around 5 μm in crystalline silicon,[37] ~1/20 of the thickness of our wafers.

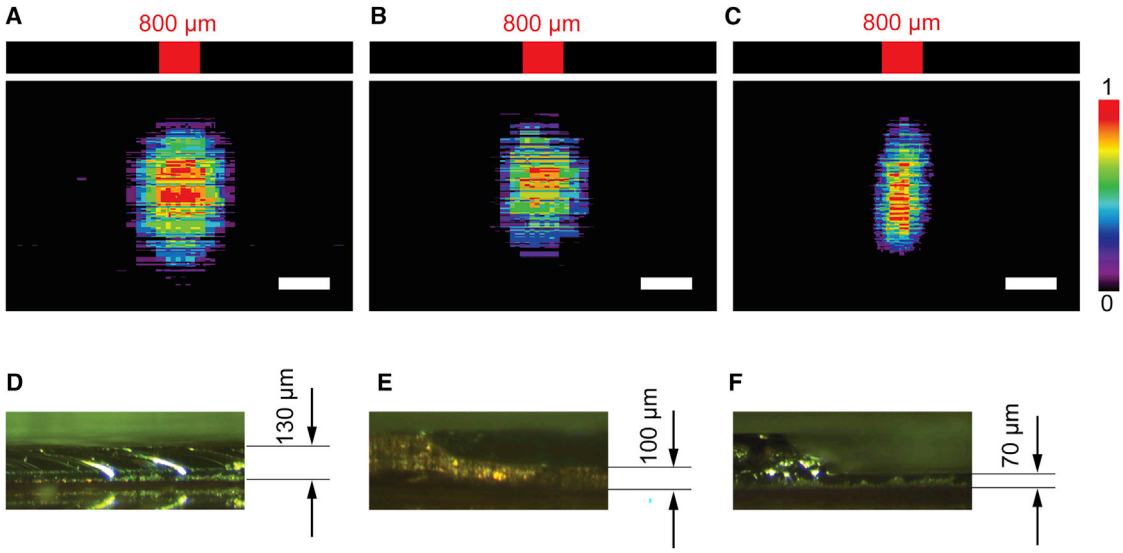

Figure 5. Spatially Resolved Electrochemiluminescence Guided on a Si Photoanode under Effectively Dark Conditions

(A–C) False-color intensity electrochemiluminescence emission maps as a function of the substrate thickness (130 μm, 100 μm and 70 μm, respectively), recorded with an exposure time of 500 ms. Intensity bar is in arbitrary units. A constant voltage of +0.8 V (versus Ag/AgCl, KCl_{sat}) was applied to the Si electrodes during the experiments. The red light (625 nm) images projected on the backside of the electrode are lines 800 μm in width and are depicted to scale (horizontal direction) above of each emission image. The electrodes, low doped n-type Si(100) substrates, were thinned by etching in 30% potassium hydroxide and modified with a monolayer of 1,8-nonadiyne. The electrolytic solution contained 1.0×10^{-1} M potassium hydroxide, 5.0×10^{-2} M luminol, and 1% (v/v) H_2O_2.

(D–F) Optical micrographs of the substrate cross-section showing the thickness of the electrodes in (A)–(C), respectively. Scale bars in (A)–(C) are 1 mm.

A first challenge when using backside illumination to assist a photoelectrochemical reaction is to minimize the loss of photogenerated carriers during their diffusion from the generation site to the wet interface. Carriers diffuse isotropically in the bulk of the electrode before reaching the space-charge layer near the semiconductor-liquid interface.[38] Therefore, the extent to which the chemiluminescence can match the geometry of the light stimulus may depend inversely on substrate thickness. For instance, we could not detect any emission when using 500 μm thick silicon wafers. Substrates below 200 μm started showing chemiluminescence, but the 2D chemiluminescence localization was only observed for even thinner substrates. Figure 5A shows an electrochemiluminescence emission image obtained by projecting a "line" pattern on the backside of a 130 μm thick substrate. The spatial resolution is significantly poorer than when using frontside illumination, but when the substrate is thinned further (100 and 70 μm, Figures 5B and 5C, respectively) the optical output becomes a better match of the excitation light pattern that is projected on the dry backside of the electrode.

We have developed the spatiotemporal control of electrochemiluminescence on single crystal silicon wafers. The electrochemiluminescence of luminol was guided in 2D and time by using visible light to generate transient arrays of microscopic electron-sink sites on an unstructured macroscopic silicon electrode. A ferroelectric micromirror spatial light modulator enables creating dynamic or static illumination patterns with high temporal resolution and absolute geometric flexibility. For instance, sequential illumination of non-adjacent electrode areas removes the speed constrains generally imposed by a raster scan, such as when mechanical moving probes are involved. This photoelectrocatalytic system on silicon shows onset of electrogenerated chemiluminescence at an unprecedented low anodic voltage, as well as upconversion from red to blue of the excitation wavelength. It opens up new prospects

in optical microscopy, with some specific advantages over fluorescence. Specifically, contrary to fluorescence, a light stimulus can address electrochemiluminescence of a sample hitting the electrode backside (air-solid interface) ensuring the electrode-liquid interface remains under complete dark conditions. This can be advantageous for photosensitive samples, as well as removing nonspecific signals, two of the main drawbacks of fluorescence dyes.

EXPERIMENTAL PROCEDURES

Resource Availability

Lead Contact

Further information and requests for resources and reagents should be directed to and will be fulfilled by the lead contact, Simone Ciampi (simone.ciampi@curtin.edu.au).

Materials Availability

This study did not generate new unique reagents.

Data and Code Availability

This study did not generate any unpublished custom code.

Chemicals and Materials

Unless specified otherwise, all chemicals were of analytical grade and used as received. Sulfuric acid (H_2SO_4, Puriss, 95%–97%, Honeywell Fluka), hydrogen peroxide (H_2O_2, MOS Puranal, 30%, Sigma Aldrich), gallium-indium eutectic (99.99%, Sigma Aldrich) 1,8-nonadiyne (98%, Sigma Aldrich), luminol (97%, Sigma Aldrich), 2-propanol (99.5%, Ajax Finichem), and sodium hydroxide (95%, Ajax Finichem) were of analytical grade and used as received. Dichloromethane was distilled before use. Milli-Q water (>18 MΩ cm) was used for surface cleaning and for preparing solutions. Prime-grade, single-side-polished silicon wafers were purchased from Siltronix, S.A.S. (Archamps, France), and unless otherwise specified they were 500 μm thick. Wafers were either (111)-oriented (±0.5°) of p-type (boron-doped, 0.007–0.013 Ω cm in resistivity), referred as highly doped (HD) or (100)- and (111)-oriented (±0.5°), n-type (phosphorous-doped, 7–13 Ω), referred as low doped (LD).

Preparation of the Amorphous Silicon Substrates

Amorphous silicon films (1 μm thick) were grown by plasma-enhanced chemical vapor deposition on Si(100) wafers (n-type, boron-doped, and 0.001–0.003 Ω cm). Prior to deposition of the amorphous silicon layer, the Si(100) substrates were cleaned in an ozone chamber, immersed for 3 min in 3% aqueous hydrofluoric acid solutions, and then blown dried under a flow of nitrogen gas.

Surface Functionalization

All silicon samples were functionalized with monolayers of 1–8 nonadiyne by a UV-assisted hydrosilylation reaction, according to a previously reported procedure.[38] In brief, silicon wafers were cut into 1 × 1 cm samples, cleaned with dichloromethane, 2-propanol and water, and then immersed in a hot Piranha solution (100°C, 1:3 H_2O_2:H_2SO_4) for 20 min. Samples were then rinsed thoroughly with Milli-Q water before being etched for 10 min in a deoxygenated 40% wt aqueous NH_4F solution. Hydrogen-terminated silicon samples were then rinsed with water and dichloromethane and then blown dry under an argon gas stream. Samples were then immediately placed on a glass slide with their polished side facing upward. A small amount (~50 μL) of deoxygenated 1,8-nonadiyne was dropped on the silicon sample. A quartz slide was placed on the sample to limit the diyne evaporation. The

hydrosilylation reaction (2 h) was carried out at room temperature, under argon, with the silicon sample kept ~200 mm away from the UV source (Vilber, model VL-215.M, 312 nm, and nominal power output of 30 W). The monolayer-modified samples were then rinsed thoroughly with dichloromethane before analysis.

Chemical Micromachining of the Silicon Electrodes

Prior to the surface functionalization (previous section), the thickness of samples used in backside illumination experiments was reduced below 200 μm by chemical etching in potassium hydroxide aqueous solutions (30% [v/v]). Thin samples were required in backside illumination in order to improve the spatial resolution of the electrochemiluminescent output. Single-side-polished Si(100), n-type (phosphorous-doped, 7–13 Ω), 200 μm thick wafers were cut into pieces of 1 × 1 cm and placed in a polytetrafluoroethylene etching cell, with the unpolished side contacting the etching solution. Samples were kept in the etching bath, set to 40°C, for either 16, 20, or 26 h, to yield, respectively, 130, 100, and 70 μm thick wafers. The exact thickness of each sample was measured with an optical microscope.

Spectroelectrochemistry

Spectral information cannot be unambiguously extracted from the RGB channels of a CMOS camera. Luminol emission spectra (e.g., Figure 2A) were therefore recorded on a Cary Eclipse Fluorescence spectrophotometer, with the Si(111) HD surfaces as the working electrode, a platinum wire as the counter electrode, and a Ag/AgCl/KCl (sat.) as the reference electrode. All electrochemical measurements were performed using a potentiostat from PalmSens BV (EmStat3).

Electrochemiluminescence Characterization and Mapping

The electrochemiluminescence emission intensity of the silicon electrodes was recorded and mapped using a CMOS camera (CS235CU, Thorlabs) and analyzed from the RGB channels in ImageJ. Experiments were performed in a three-electrode electrochemical cell (Figure S3) with an Ag/AgCl (sat. KCl) as the reference electrode, an ITO slide (ITO on glass, 8–12 Ω/sq., Delta Technologies) as the counter electrode and the silicon substrates as the working electrode. All potentials are reported versus the reference electrode. The backside of the silicon substrate was pressed against a copper plate and ohmic contact was ensured by applying a small amount of gallium-indium eutectic between the silicon and the copper plate. A small hole (⌀ 6 mm) in the center of the plate allowed for the excitation light to reach the silicon backside. All electrochemical measurements were performed using an EmStat3 potentiostat. The spatiotemporal resolution of the electrochemiluminescence emission was attained using a microprojection system to localize the incident light on the silicon substrate (Figure 1D and Figure S4). This illumination system is built around a ferroelectric liquid crystal on silicon (FLCoS) spatial light modulator (QXGA-3DM, Forth Dimension Displays, 3.1 MPixel), as schematized in Figure 1D. A deep red LED (730 nm, M730L5, Thorlabs, nominal power 680 mW) was used as the light source for experiments with frontside (silicon-electrolyte interface) illumination. For experiments under backside illumination (air-silicon interface) a red LED (625 nm, M625L3, Thorlabs, nominal power 770 mW) was used. The LED light was collimated and *s*-polarized (LPVISC100, Thorlabs) before hitting the FLCoS micromirror. Depending on the ON-OFF status of each pixel of the micromirror, the polarization remained either unchanged (OFF pixels) or was converted to *p*-polarized (ON pixels). The *s* polarization was reflected and lost, while the *p* polarization was allowed to pass through a beam splitter (CM1-PBS251, Throlabs, for backside illumination and CCM1-PBS252, Thorlabs, for frontside illumination) and focused (AF-S NIKKOR, Nikon, 50 mm, f/1.8G) either on the semiconductor-electrolyte or air-semiconductor

interfaces. The electrochemiluminescence emission was reflected by a dichroic mirror toward the CMOS camera, after passing through a focusing lens (MVL50M23, Thorlabs, 50 mm, f/2.8). The experimental setup varied slightly depending on the illumination side (frontside versus backside, Figure 1D). All experiments were performed inside a light-proof Faraday cage. Backside experiments were performed using Si(100) electrodes, while Si(111) was used for the frontside experiments.

The projected images were uploaded as bitmap files to the QXGA-3DM PCB. The bitmap files were generated in MATLAB. The specific sequence and projecting time of the images were specified by the QXGA-3DM user interface.

SUPPLEMENTAL INFORMATION

Supplemental Information can be found online at https://doi.org/10.1016/j.xcrp.2020.100107.

ACKNOWLEDGMENTS

This work was financially supported by the Australian Research Council (DP190100735 [S.C. and N.D.] and FT190100148 [S.C.]).

AUTHOR CONTRIBUTIONS

Y.B.V. performed the experiments and analyzed the data. S.C. and Y.B.V. conceived the idea and developed the methodology. S.C. supervised the project. N.D. provided useful discussions on semiconductor electrochemistry. All authors wrote the manuscript.

DECLARATION OF INTERESTS

The authors declare no competing interests.

Received: March 28, 2020
Revised: May 16, 2020
Accepted: May 28, 2020
Published: July 8, 2020

REFERENCES

1. Miao, W. (2008). Electrogenerated chemiluminescence and its biorelated applications. Chem. Rev. *108*, 2506–2553.
2. Campbell, A.K. (1988). Chemiluminescence: Principles and Applications in Biology and Medicine (Ellis Horwood).
3. Durrant, I. (1990). Light-based detection of biomolecules. Nature *346*, 297–298.
4. Denk, W., Strickler, J.H., and Webb, W.W. (1990). Two-photon laser scanning fluorescence microscopy. Science *248*, 73–76.
5. Lichtman, J.W., and Conchello, J.-A. (2005). Fluorescence microscopy. Nat. Methods *2*, 910–919.
6. Hell, S.W., and Wichmann, J. (1994). Breaking the diffraction resolution limit by stimulated emission: stimulated-emission-depletion fluorescence microscopy. Opt. Lett. *19*, 780–782.
7. Créton, R., and Jaffe, L.F. (2001). Chemiluminescence microscopy as a tool in biomedical research. Biotechniques *31*, 1098–1100, 1102–1105.
8. Vogel, Y.B., Gooding, J.J., and Ciampi, S. (2019). Light-addressable electrochemistry at semiconductor electrodes: redox imaging, mask-free lithography and spatially resolved chemical and biological sensing. Chem. Soc. Rev. *48*, 3723–3739.
9. Zhao, Y., Yu, J., Xu, G., Sojic, N., and Loget, G. (2019). Photoinduced Electrochemiluminescence at Silicon Electrodes in Water. J. Am. Chem. Soc. *141*, 13013–13016.
10. Dodeigne, C., Thunus, L., and Lejeune, R. (2000). Chemiluminescence as diagnostic tool. A review. Talanta *51*, 415–439.
11. Xu, J., Huang, P., Qin, Y., Jiang, D., and Chen, H.Y. (2016). Analysis of Intracellular Glucose at Single Cells Using Electrochemiluminescence Imaging. Anal. Chem. *88*, 4609–4612.
12. Huo, X.-L., Yang, H., Li, M.-X., Zhao, W., Xu, J.-J., Wang, Y., Luo, X.-L., and Chen, H.-Y. (2018). Multi-segmented CdS-Au nanorods for electrochemiluminescence bioanalysis. Nanoscale *10*, 19224–19230.
13. Finklea, H.O. (1988). Semiconductor Electrodes (Elsevier).
14. Haapakka, K.E., Kankare, J.J., and Jyrki, A.L. (1982). Determination of the second acidity constant of luminol. Anal. Chim. Acta *139*, 379–382.
15. Knight, A.W., and Greenway, G.M. (1994). Occurrence, mechanisms and analytical applications of electrogenerated chemiluminescence. A review. Analyst (Lond.) *119*, 879–890.
16. Vogel, Y.B., Gonçales, V.R., Gooding, J.J., and Ciampi, S. (2018). Electrochemical Microscopy

based on Spatial Light Modulators: A Projection System to Spatially Address Electrochemical Reactions at Semiconductors. J. Electrochem. Soc. *165*, H3085–H3092.

17. Chen, B.-C., Legant, W.R., Wang, K., Shao, L., Milkie, D.E., Davidson, M.W., Janetopoulos, C., Wu, X.S., Hammer, J.A., 3rd, Liu, Z., et al. (2014). Lattice light-sheet microscopy: imaging molecules to embryos at high spatiotemporal resolution. Science *346*, 1257998.

18. Vogel, Y.B., Gonçales, V.R., Al-Obaidi, L., Gooding, J.J., Darwish, N., and Ciampi, S. (2018). Nanocrystal Inks: Photoelectrochemical Printing of Cu_2O Nanocrystals on Silicon with 2D Control on Polyhedral Shapes. Adv. Funct. Mater. *28*, 1804791.

19. Vogel, Y.B., Zhang, J., Darwish, N., and Ciampi, S. (2018). Switching of Current Rectification Ratios within a Single Nanocrystal by Facet-Resolved Electrical Wiring. ACS Nano *12*, 8071–8080.

20. Choudhury, M.H., Ciampi, S., Yang, Y., Tavallaie, R., Zhu, Y., Zarei, L., Gonçales, V.R., and Gooding, J.J. (2015). Connecting electrodes with light: one wire, many electrodes. Chem. Sci. (Camb.) *6*, 6769–6776.

21. Fang, C., Li, H., Yan, J., Guo, H., and Yifeng, T. (2017). Progress of the Electrochemiluminescence Biosensing Strategy for Clinical Diagnosis with Luminol as the Sensing Probe. ChemElectroChem *4*, 1587–1593.

22. Ciampi, S., Eggers, P.K., Le Saux, G., James, M., Harper, J.B., and Gooding, J.J. (2009). Silicon (100) electrodes resistant to oxidation in aqueous solutions: an unexpected benefit of surface acetylene moieties. Langmuir *25*, 2530–2539.

23. Choudhury, M.H., Ciampi, S., Lu, X., Kashi, M.B., Zhao, C., and Gooding, J.J. (2017). Spatially Confined Electrochemical Activity at a Non-Patterned Semiconductor Electrode. Electrochim. Acta *242*, 240–246.

24. Vogel, Y.B., Darwish, N., Kashi, M.B., Gooding, J.J., and Ciampi, S. (2017). Hydrogen Evolution during the Electrodeposition of Gold Nanoparticles at Si(100) Photoelectrodes impairs the Analysis of Current-Time Transients. Electrochim. Acta *247*, 200–206.

25. Vogel, Y.B., Molina, A., Gonzalez, J., and Ciampi, S. (2019). Quantitative Analysis of Cyclic Voltammetry of Redox Monolayers Adsorbed on Semiconductors: Isolating Electrode Kinetics, Lateral Interactions, and Diode Currents. Anal. Chem. *91*, 5929–5937.

26. Santangelo, P.G., Miskelly, G.M., and Lewis, N.S. (1989). Voltammetry of Semiconductor Electrodes. 2. Cyclic Voltammetry of Freely Diffusing Redox Species and Rotating Semiconductor Disk Voltammetry. J. Phys. Chem. *93*, 6128–6136.

27. Santangelo, P.G., Miskelly, G.M., and Lewis, N.S. (1988). Cyclic Voltammetry at Semiconductor Photoelectrodes. 1. Ideal Surface-Attached Redox Couples with Ideal Semiconductor Behavior. J. Phys. Chem. *92*, 6359–6367.

28. Vogel, Y.B., Zhang, L., Darwish, N., Gonçales, V.R., Le Brun, A., Gooding, J.J., Molina, A., Wallace, G.G., Coote, M.L., Gonzalez, J., and Ciampi, S. (2017). Reproducible flaws unveil electrostatic aspects of semiconductor electrochemistry. Nat. Commun. *8*, 2066.

29. George, M., Parak, W.J., Gerhardt, I., Moritz, W., Kaesen, F., Geiger, H., Eisele, I., and Gaub, H.E. (2000). Investigation of the Spatial Resolution of the Light-Addressable Potentiometric Sensor. Sens. Actuators A Phys. *86*, 187–196.

30. Moritz, W., Yoshinobu, T., Finger, F., Krause, S., Martin-Fernandez, M., and Schöning, M.J. (2004). High Resolution LAPS Using Amorphous Silicon as the Semiconductor Material. Sens. Actuators B Chem. *103*, 436–441.

31. Nikolenko, V., Watson, B.O., Araya, R., Woodruff, A., Peterka, D.S., and Yuste, R. (2008). SLM Microscopy: Scanless Two-Photon Imaging and Photostimulation with Spatial Light Modulators. Front. Neural Circuits *2*, 5.

32. Lutz, C., Otis, T.S., DeSars, V., Charpak, S., DiGregorio, D.A., and Emiliani, V. (2008). Holographic photolysis of caged neurotransmitters. Nat. Methods *5*, 821–827.

33. Wu, F., Zhou, B., Wang, J., Zhong, M., Das, A., Watkinson, M., Hing, K., Zhang, D.-W., and Krause, S. (2019). Photoelectrochemical Imaging System for the Mapping of Cell Surface Charges. Anal. Chem. *91*, 5896–5903.

34. Polcari, D., Dauphin-Ducharme, P., and Mauzeroll, J. (2016). Scanning Electrochemical Microscopy: A Comprehensive Review of Experimental Parameters from 1989 to 2015. Chem. Rev. *116*, 13234–13278.

35. Baltes, N., Thouin, L., Amatore, C., and Heinze, J. (2004). Imaging concentration profiles of redox-active species with nanometric amperometric probes: effect of natural convection on transport at microdisk electrodes. Angew. Chem. Int. Ed. Engl. *43*, 1431–1435.

36. Liu, X., Ramsey, M.M., Chen, X., Koley, D., Whiteley, M., and Bard, A.J. (2011). Real-time mapping of a hydrogen peroxide concentration profile across a polymicrobial bacterial biofilm using scanning electrochemical microscopy. Proc. Natl. Acad. Sci. USA *108*, 2668–2673.

37. Green, M.A., and Keevers, M.J. (1995). Optical Properties of Intrinsic Silicon at 300 K. Prog. Photovolt. Res. Appl. *3*, 189–192.

38. Zhang, Q. (2005). Theoretical Analysis and Design of Submicron-LAPS. Sens. Actuators B Chem. *105*, 304–311.